Astronomy
&
Astrophysics

Investigation of a sample of carbon-enhanced metal-poor stars observed with FORS[*] and GMOS[**],[***]

E. Caffau[1], A. J. Gallagher[2,1], P. Bonifacio[1], M. Spite[1], S. Duffau[3], F. Spite[1], L. Monaco[3], and L. Sbordone[4]

[1] GEPI, Observatoire de Paris, Université PSL, CNRS, 5 Place Jules Janssen, 92190 Meudon, France
  e-mail: elisabetta.caffau@obspm.fr
[2] Max-Planck-Institut für Astronomie, Königstuhl 17, 69117 Heidelberg, Germany
[3] Departamento de Ciencias Fisicas, Universidad Andres Bello, Fernandez Concha 700, Las Condes, Santiago, Chile
[4] European Southern Observatory, Casilla 19001, Santiago, Chile

ABSTRACT

Aims. Carbon-enhanced metal-poor (CEMP) stars represent a sizeable fraction of all known metal-poor stars in the Galaxy. Their formation and composition remains a significant topic of investigation within the stellar astrophysics community.
Methods. We analysed a sample of low-resolution spectra of 30 dwarf stars, obtained using the visual and near UV FOcal Reducer and low dispersion Spectrograph for the Very Large Telescope (FORS/VLT) of the European Southern Observatory (ESO) and the Gemini Multi-Object Spectrographs (GMOS) at the GEMINI telescope, to derive their metallicity and carbon abundance.
Results. We derived C and Ca from all spectra, and Fe and Ba from the majority of the stars.
Conclusions. We have extended the population statistics of CEMP stars and have confirmed that in general, stars with a high C abundance belonging to the high *C* band show a high Ba-content (CEMP-s or -r/s), while stars with a normal C abundance or that are C-rich, but belong to the low *C* band, are normal in Ba (CEMP-no).

Key words. stars: Population II – stars: abundances – Galaxy: abundances – Galaxy: formation – Galaxy: halo

1. Introduction

The existence of stars with large carbon enhancement was suspected from the very beginning of astronomical spectroscopy. In his "Memoria" of 1868, Angelo Secchi (Secchi 1868) added a fourth spectral type to the three he defined earlier and noted that "not all the stars of the fourth type have identical spectra: this type allows a wider variety than the three previous ones. The black line after the green almost coincides with magnesium, but it may well be due to carbon. More precise measures will decide: its width makes us believe that it is not metallic"[1]. The "black line" observed by Secchi is indeed the C_2 Swan band that characterises carbon stars, i.e. stars that have C/O[2] > 1, see

McCarthy (1994) for more details on Secchi's discovery and a modern identification of his type 4 stars. It is remarkable that at the low resolution of his prism spectra, Secchi was able to suspect that the line was too wide to be an atomic line; this proves that Secchi was an exceptional observer.

In what can be considered a milestone review, Bidelman (1956) introduced the class of "non-typical" carbon stars, and among these the "CH stars" that show "extremely strong features due to CH, and considerably weaker lines of neutral metals than do the "typical" carbon stars". This was the first class of metal-poor carbon-enhanced stars to be clearly identified, although they are only "mildly" metal poor ([Fe/H] ≳ −1.5). As soon as it was possible to determine detailed chemical abundances, it became clear that the composition of carbon stars was the result of nuclear processing; this concept is well explained in the influential review by Wallerstein (1973). At the time it was unclear, however, whether this processing took place in the star itself (self-pollution) or if it was the result of mass transfer from an evolved companion. By the mid-1990s, the general consensus was that Ba stars, CH-stars, and sg-CH-stars were the result of mass transfer in a binary system (McClure 1984, 1997, McClure & Woodsworth 1990). During its lifetime, the higher mass star of the binary system evolves onto the asymptotic giant branch (AGB), where it is fuelled in part by helium burning, producing freshly synthesised carbon and dredging it up to its atmosphere through several convective mechanisms, induced by thermal pulsations. The giant star atmosphere then expands and becomes tenuous, exceeding its Roche lobe or even encompassing the lower mass companion in the case of close binary systems. This allows accretion of the atmosphere of the

---

[1] Original text in Italian: "Non tutte le stelle del 4° tipo sono di spettro identico: questo tipo ammette varietà maggiori che i tre precedenti.
La riga nera dopo il verde coincide quasi con il magnesio, ma può bene anche appartenere al carbonio. Le misure più precise decideranno: la sua larghezza ci fa credere che non è la metallica".
[2] $X/Y = N(X)/N(Y) = 10^{[A(X)_* - A(Y)_*]}$.

higher mass star, which contains freshly synthesised carbon, by the lower mass star.

The HK survey (Beers et al. 1985, 1992) was aimed at the discovery of metal-poor stars. One of the first surprising results was that about 10% of the stars with an estimated metallicity below –2.0 showed a G-band stronger than normal, while at higher metallicity, strong G-band stars were less frequent (Norris et al. 1997a). The first handful of strong G-band stars from the HK Survey that were analysed at high resolution proved to be enhanced in the s-process elements (Barbuy et al. 1997; Norris et al. 1997a), and the exceptional star CS 22892-052 proved to be also enhanced in r-process elements (McWilliam et al. 1995; Sneden et al. 1996). This was a strong suggestion that these stars are indeed metal-poor analogues of CH-stars and the result of mass-transfer in a binary system. The situation changed drastically with the study of CS 22957-027 (Norris et al. 1997b; Bonifacio et al. 1998), which showed a large C-enhancement and a very strong Swan band (Bonifacio et al. 1998), but no enhancement of any of the neutron capture elements. In order to distinguish these stars from the classical carbon stars and CH-stars, it soon become customary to refer to them as carbon-enhanced metal-poor stars (CEMP, for short); the first two occurrences of the acronym in the literature are in Lucatello et al. (2003) and in the review by Christlieb (2003).

We take the definition of Beers & Christlieb (2005), and consider a metal-poor star as a CEMP when [Fe/H] $\lesssim -2.0$ dex and [C/Fe] $> +1.0$ dex. When a CEMP star is also enhanced in $s-$process elements, we refer to it as a CEMP-s star, i.e. [C/Fe] $> +1.0$, [Ba/Fe] $> +1.0$ and [Ba/Eu] $> +0.5$ (Beers & Christlieb 2005). Another sub-class of CEMP stars show enhancements in both slow (s-) and rapid (r-) process material, such that [C/Fe] $> +1.0$ and $0.0 <$ [Ba/Eu] $< +0.5$ (Beers & Christlieb 2005). These stars are referred to as CEMP-r/s stars. Like CEMP-s stars, a large fraction of CEMP-r/s stars are found in binary systems, explaining their carbon and s-process enhancements. The r-process enhancement is peculiar, however. It has been suggested that these stars undergo a double-enhancement phase (Jonsell et al. 2006; Bisterzo et al. 2006). The s-process and carbon enhancement still occurs due to binary interaction, but the r-process enhancement takes place in the forming gas cloud, when it is enriched by r-process material. Since the discovery of GW170817 (Troja et al. 2017), observational evidence suggests that the main sites for the r-process are neutron star mergers. The r-process-rich ejecta from these events mix with the interstellar medium (ISM), which will become star-forming regions and form new generations of r-rich stars. Moreover, Hampel et al. (2016) could explain the pattern of the heavy element abundances in 20 CEMP-rs stars by the accretion of the products of the i-process (Cowan & Rose 1977) occuring in the intershell region of low-metallicity AGB stars.

CEMP-s (and CEMP-r/s) stars are the most commonly found sub-class of CEMP stars, making up approximately 80% of all CEMP stars known (Aoki et al. 2007, 2008). It is now well established that the CEMP-s stars are all members of binary systems (Lucatello et al. 2005; Starkenburg et al. 2014). However, some CEMP stars appear to be similar to the prototype star CS 22957-027 and show no other enhancements. These stars are known as CEMP-no stars ([C/Fe] $> +1.0$, [Ba/Fe] < 0.0 Beers & Christlieb 2005). Additionally, there is currently no evidence that supports an unusually high fraction of binarity in these objects, but only a handful of these objects have radial velocity measurements at this time (e.g. the ultra Fe-poor star by Caffau et al. 2016). This would

suggest that accretion through binary interaction is probably not the means by which these stars attained their carbon enhancement. Therefore, these stars would appear to exhibit abundance patterns indicative of the gas cloud from which they formed, making their unusual chemical composition a mystery.

Spite et al. (2013) suggested that CEMP stars are divided into two groups: the high C band and the low C band. Bonifacio et al. (2015) argued for a different origin of the two groups, where the stars of the higher band are members of a binary system and those that belong to the low band present the composition of the gas cloud from where they have formed, as described above. Further thoughts on the two C bands are discussed by Bonifacio et al. (2018). In the case of dwarf CEMP stars, when they are extremely metal poor, it is in general not easy to detect any sign of heavy elements. The most Fe-poor stars known belong to the low C band, while the stars in the high C band rarely have [Fe/H] $\lesssim -3.5$ dex. Bonifacio et al. (2018) proposed a classification for the stars on the two C bands according their C abundance, regardless of their abundances in neutron capture elements.

We present an analysis made on a sample of stars observed at low resolution with the visual and near UV FOcal Reducer and low dispersion Spectrograph for the Very Large Telescope (FORS/VLT) of the European Southern Observatory (ESO) and the Gemini Multi-Object Spectrographs (GMOS) at the GEMINI telescope, in the following study, and examine, among other things, their carbon abundances.

2. Observations and data reduction

The spectra presented in this paper have been acquired in the course of two programs approved by the ESO and GEMINI observatories. The programs have been designed to be "filler" programs, meaning that they can acquire useful data in weather conditions when most programs cannot operate and have no constraint on the Moon phase. Our spectra have been acquired with FORS (Appenzeller et al. 1998) at the ESO VLT 8.2 m telescope and with GMOS (Hook et al. 2004) at the GEMINI 8.2 m telescope.

The FORS spectra have been observed in service mode during the ESO Programme 099.D-0791, between 01/04/2017 and 16/08/2017. We used GRIS 1200B with a central wavelength of 436 nm and a slit width of $0\rlap{.}''29$, which provides a resolving power $R \sim 5000$ at the central wavelength and a continuous spectral coverage in the range 366 nm to 511 nm. The detector used was the CCD mosaic of two 2k × 4k MIT CCDs with pixel size of 15 μm. The detectors are arranged in a line in the direction orthogonal to the dispersion, thus there are no gaps in the spectra. This mosaic is more sensitive in the red; using the blue sensitive mosaic of E2V CCDs would have been more efficient, but this detector camera is normally not mounted on FORS. Since the program was designed as a "filler" program, we had to use the default detector. We initially began the observations with a 2 × 2 on-chip binning, that is, the default for FORS, which is supposed to be used for service observations. We knew that in this way, the spectrum would be under-sampled in the blue part, but our primary goal was the G-band, which is very wide and thus would not be under-sampled; the same applies to the Ca II K line.

We acquired spectra for eight stars in this configuration (SDSS J0905+0330, SDSS J1248–0726, SDSS J1313–0019, SDSS J1349–0229, SDSS J1411+0503, SDSS J2137–0057, SDSS J2219+0515, and SDSS J2239–0048). As soon as the

spectra were observed, they were reduced with the ESO FORS pipeline[3] driven by gasgano[4]. They were subsequently analysed with MyGIsFOS (Sbordone et al. 2014). At this point, we realised that several Fe I lines could be used in the blue part of the spectrum and that the under-sampling introduced an undesirable increase in the uncertainty. We therefore submitted to ESO a waiver request to be allowed to use the 1×1 binning even in service mode. The waiver was approved and all subsequent observations were acquired with a 1×1 binning. For each star we used an observing block of 1 h. For the 2×2 binning, this translates into an effective exposure time of 2829 s. For the 1×1 binning, since the read-out time is longer, this translates into 2762 s of exposure time. Thirty spectra of quality A or B and one spectrum with quality C have been retained for analysis for a total of 28 stars. Star SDSS J144533.32–004559.0 had two "B" quality spectra, each of which was analysed independently.

The GMOS spectra were acquired in service mode on the nights of 21/07/2017 and 25/07/2017. We used the B1200+_G5321 grating centred at 468 nm, with a slit of $0\rlap{.}''5$. This combination provides a resolving power $R = 3744$ at the blaze wavelength (463 nm) and a spectral coverage from 387 nm to 548 nm. The detector was a mosaic of three Hamamatsu $2\,\mathrm{k} \times 4\,\mathrm{k}$ CCDs with pixels of $15\,\mu\mathrm{m}$ side (Gimeno et al. 2016). The three detectors are arranged in a line along the dispersion direction, which implies that there are two gaps in the wavelength range. The gap ranges are $438.7-440.8$ nm and $493.0-495.1$ nm. We used a 2×2 binning, which is the default. For each star we observed three exposures of 441 s. The data were processed with GEMINI IRAF[5] package[6], to perform bias subtraction, flat-fielding, and mosaicking of the different sub-images. We then used the ESO MIDAS[7] LONG context to perform the wavelength calibration using the CuAr lamp spectra and the optimal extraction (including sky-subtraction). The three exposures for each star where then added and analysed with MyGIsFOS.

3. Sample

We selected a sample of turn-off stars from the Sloan Digital Sky Survey (SDSS; York et al. 2000; Yanny et al. 2009) that were bright enough ($g < 17$) to allow us to secure a reasonable spectrum quality in a single observing block of 1 h. To select turn-off stars on the SDSS, we requested $0.18 \leq (g - z)_0 \leq 0.70$ and $(u - g)_0 > 0.70$ (see Caffau et al. 2013b) and obtained a sample of about 20 000 stars observable from Paranal. By examining our own analysis of the SDSS spectra, we focused on stars for which we derived a metallicity in the range $-3.0 < [\mathrm{Fe/H}] < -0.5$ and that also exhibited a strong G-band features. This meant that stars that potentially belonged to either C bands (Spite et al. 2013) were selected, as well as stars at the metal-rich end of the two C bands – "normal" stars, with a solar-scaled C abundance.

Table 1 lists the stars we examined here, along with their coordinates, g-mag, and metallicities derived from Fe abundances computed using SDSS and FORS/GMOS spectra.

---

[3] ftp://ftp.eso.org/pub/dfs/pipelines/fors/fors-kit-5.3.23.tar.gz
[4] ftp://ftp.eso.org/pub/dfs/gasgano/gasgano-2.4.8.tar.gz
[5] http://iraf.noao.edu/
[6] http://www.gemini.edu/node/11823
[7] https://www.eso.org/sci/software/esomidas/

4. Analysis

4.1. Comparison FORS/GMOS - SDSS

In the FORS and GMOS spectra, several Fe I lines are usually available to derive A(Fe) (and also [Fe/H]). However, we were not able to derive a direct Fe abundance for three stars (SDSS J2219+0515, SDSS J1149+0723, and SDSS J1349–0229) because no clean Fe line was available in their spectra. Instead, we provide an estimation of A(Fe) based on comparison of synthetic spectra and observed on the full spectral range. For these stars, the σ related to the iron abundance is an estimation of the uncertainty in this comparison.

The SDSS spectra are of lower resolution, and in this case, we derive the metallicity, [M/H], from any available metallic feature in the spectra, so that the metallicity is usually based on Ca, Mg, and Fe abundances. The synthetic spectra we used for the chemical investigation of the SDSS spectra are enhanced in α elements by +0.4 dex in the metal-poor regime, as normally expected in Galactic metal-poor stars. So the scale provided to give the metallicity, [M/H], is related to the Fe abundance. This is reasonable for "normal" stars that do not show peculiar [Mg/Fe] or [Ca/Fe] ratios, which seems to be mainly the case in this sample of stars. In Table 1 we list the [Fe/H] derived from the FORS and GMOS spectra and the [M/H] from the SDSS spectra. The comparison is generally very good, but there are some exceptions that we discuss below. When multiple SDSS spectra of comparable quality were available, the metallicity and the uncertainty listed in Table 1 represent an average value.

Nineteen of the 27 stars in the sample present absolute differences in the metallicity derived from SDSS and the iron content from the FORS and GMOS spectra lower than 0.3 dex, and for 22 stars, this is lower than 0.5 dex. For all but three spectra (SDSS J1349–0229, SDSS J2137–0057, and SDSS J1411+0503), the metallicity from SDSS and [Fe/H] from FORS/GMOS spectra agree within the uncertainties.

We present some of the more interesting facts about a small number of the stars we analysed in Table 1.

– SDSS J1349–0229 shows the largest difference in metallicity when the FORS and SDSS spectra are analysed. Two spectra are available in SDSS DR12, providing a large difference among themselves in metallicity of 0.65 dex. For one of them, the metallicity is based on a single line. We report in Table 1 the metallicity derived from the other SDSS spectrum, based on four features, still with a large uncertainty. In addition, the quality of the FORS spectrum is not good (classified as "C") and is the poorest FORS spectrum in our sample. The difference in the [M/H] from the best SDSS spectrum and [Fe/H] from the FORS spectrum is 1.44 dex, just larger than the sum of the two uncertainties (1.38 dex). SDSSJ1349–0229 was also analysed by Behara et al. (2010) with a temperature only 62 K hotter than the value given in Table 2. We derived from the FORS spectra the same Fe abundance as Behara et al. (2010), and we consider the results of the two analyses in very good agreement.

– The metallicity and [Fe/H] derived from SDSS and FORS spectra, respectively, for SDSS J2137–0057 differ by 0.63 dex, but the uncertainties are 0.60 dex, so the agreement is acceptable.

– The difference in metallicity and [Fe/H] in SDSS J1411+0503 from SDSS and FORS spectra is 0.8 dex with uncertainties of 0.62 dex. The SDSS analysis is based on two spectra, providing metallicities within 0.01 dex, and the uncertainty is 0.4 and 0.3 dex for the two spectra. One SDSS spectrum has no Ca II-K,

Table 1. Sample of stars.

Star	RA $_\circ$	Dec $_\circ$	g^a	MJD	VR $_{SDSS}$	σ	VR	σ	[M/H] $_{SDSS}$	σ	[Fe/H]	σ
FORS												
SDSS J001547.45+001326.6	3.9477144	+0.22406663	15.81	57953.33251196	−20	2^a	−10	20	−0.75	0.24	−0.70	0.17
SDSS J004036.97+002540.7	10.154042	+0.42797715	16.29	57953.37109608	+82	3	+92	19	−1.99	0.22	−1.99	0.21
SDSS J004252.51+005521.8	10.718813	+0.92273976	16.83	57956.28170347	−256	4	−270	29	−1.70	0.24	−1.65	0.13
SDSS J022226.20−031338.0	35.609189	−3.2272445	16.95	57956.32784048	−124	3	−90	32	−2.22	0.49	−2.63	0.24
SDSS J030929.93+054246.4	47.374692	+5.7129120	15.25	57966.32655116	−82	2	−57	35	−0.96	0.26	−0.96	0.16
SDSS J034635.17−055818.3	56.64657	−5.9717720	16.96	57973.36030252	+19	2	+32	27	−1.20	0.26	−0.85	0.19
SDSS J090536.50+033034.5	136.40208	+3.5096110	16.86	57852.99994682	+272	4	+295	21	−2.19	1.03	−3.12	0.21
SDSS J114932.51+072347.0	177.38547	+7.3963985	16.34	57953.98955476	−15	3	−33	34	−2.88	0.15	$−2.82^b$:	0.40
SDSS J124841.09−072646.6	192.17123	−7.4462930	16.84	57845.30650769	−7	3	−45	26	−1.28	0.45	−1.64	0.39
SDSS J131550.68+172707.0	198.96119	+17.451962	16.12	57940.06317480	+306	3	+315	34	−2.22	0.67	−2.52	0.06
SDSS J133704.70+083523.4	204.26961	+8.5898340	16.06	57951.97732700	−21	3	−19	23	−1.38	0.15	−1.31	0.17
SDSS J133750.48+083610.8	204.46034	+8.6030160	16.72	57952.02268752	+7	3	+16	28	−0.99	0.37	−0.78	0.18
SDSS J133753.36+083734.2	204.47237	+8.6261760	15.78	57955.06167568	−34	3	−11	34	−0.51	0.26	−0.45	0.25
SDSS J133802.22+083056.2	204.50927	+8.5156120	16.93	57956.00287188	−19	3	−10	27	−0.51	0.51	−0.53	0.18
SDSS J134247.69+083521.0	205.69872	+8.5891910	15.54	57981.98808043	−42	4	−23	31	−1.63	0.18	−1.48	0.23
SDSS J134343.08+081029.3	205.92952	+8.1748110	14.92	57981.98808043	−13	2	−4	34	−0.47	0.36	−0.50	0.22
SDSS J134913.54−022942.8	207.30642	−2.4952258	16.64	57916.14995942	+140	3	+128	27	−1.58	0.98	$−3.02^b$:	0.40
SDSS J141123.09+050345.6	212.84622	+5.0626727	16.03	57933.97656561	−238	4	−210	25	−2.56	0.35	−3.36	0.27
SDSS J144533.32−004559.0	221.38887	−0.7663930	15.32	57941.10539190	−9	2	−13	30	−3.04	0.22	−2.94	0.19
SDSS J144533.32−004559.0	221.38887	−0.7663930	15.32	57941.13882949	−9	2	−19	30	−3.04	0.22	−2.94	0.19
SDSS J154338.58+092904.9	235.91078	+9.4847057	16.04	57952.06105676	+48	2	+53	23	−2.41		−2.38	0.23
SDSS J160646.36+052218.2	241.69318	+5.3717390	16.88	57954.10306751	−85	3	−97	22	−1.02	0.44	−1.27	0.29
SDSS J213752.52−005754.3	324.46883	−0.96510684	16.74	57915.30185193	−108	5	−73	23	−2.46	0.52	−3.09	0.08
SDSS J221911.25+051519.5	334.79691	+5.2554223	16.94	57915.34479028	−232	3	−259	24	−2.85	0.32	$−2.22^b$:	0.40
SDSS J223946.42−004827.7	339.94342	−0.8077150	15.73	57938.28656970	−145	2	−149	22	−1.24	0.45	−1.49	0.22
SDSS J231108.61+002650.3	347.78588	+0.44731512	16.77	57940.32010047	−64	3	−60	21	−1.46	0.32	−1.68	0.27
SDSS J233526.49+081905.9	353.86042	+8.3183210	16.53	57940.35885623	+32	3	+48	23	−1.35	0.12	−1.22	0.19
SDSS J233757.06+143607.2	354.48775	+14.602015	16.91	57951.22060599	−49	2	−43	38	−0.81	0.23	−0.85	0.23
SDSS J131326.89−001941.4	198.362066	−0.32766	16.87	57919.0637425								
GMOS												
SDSS J111434.26−120214.0	168.64275	−12.0372389	16.63	57955.174264249	−4	2			−0.84	0.22	−1.07	0.22
SDSS J201114.15−111003.9	302.8089583	−11.16775	16.31	57955.147332606	−102	2			−1.22	0.30	−1.03	0.17
SDSS J212351.59−080416.3	320.9649583	−8.0712167	16.73	57959.973129110	−334	4			−2.89	0.09	−2.91	0.09

Notes. [M/H] from SDSS is based on several metallic features; [Fe/H] from FORS and GMOS spectra are taken from Fe I lines only. The solar A(Fe) = 7.52 adopted is taken from Caffau et al. (2011). The σ are line-to-line scatter, and for the uncertain cases, the colon in the iron abundance is an estimate of the uncertainty in the comparison to synthetic spectra. [a] g magnitudes are those used to derive the effective temperatures and are taken from the SDSS-DR 12. [b] Estimation from comparison to synthetic spectra; we consider these measurements to be uncertain.

but other features are present. The 0.8 dex difference from SDSS and FORS spectra is just larger than 1σ, so we find it acceptable.
– For the star SDSS J2219+0515, there is a 0.63 dex difference between the metallicity derived from the SDSS spectrum and [Fe/H] derived from the FORS spectrum (which falls within the uncertainties of the two measurements) that can be explained by no-clean Fe line in the FORS spectrum. The A(Ca) value derived from the FORS data is in perfect agreement with the SDSS analysis.
– For SDSS J0905+0330, the metallicity derived from the SDSS spectrum has a large uncertainty (1 dex) and is based on only two features; as a consequence, the 0.93 dex difference with the [Fe/H] from the FORS spectrum is well within 1σ.
– For the stars SDSS J0346–0558 and SDSS J1248–0726, *Gaia* (Gaia Collaboration 2016) detected another source, 1.21 mag fainter, at distances of 5 arcsec and 4 arcsec, respectively. The difference in flux from our target star and the other

object is in both cases large enough to avoid compromising our analysis.
– SDSS J2011–1110: two objects are detected by *Gaia* within 2 arcsec, with a difference in the *Gaia* mag of 2.53. The two objects are very close, but the fainter star is too faint to interfere with the signal from our target.
– SDSS J1315+1727, SDSS J1337+0836, SDSS J1337+0836, SDSS J1337+0837, and SDSS J1343+0810 have a 2MASS identification.

4.2. Radial velocities

The radial velocities have been derived with the cross-correlation of each spectrum with a synthetic spectrum with very similar parameters, also taking into account the C enhancement of the star. We are aware that FORS suffers from the telescope flexions, which makes the radial velocity measurements uncertain. We took into account the position of the stars in the sky

Table 2. Derived abundances.

Star	T_{eff}	A(Fe)	A(FeII)	A(C)	3Dcor	A(Mg)	A(Si)	A(CaK)/A(Ca)	A(Ti)	A(Mn)	A(Sr)	A(Ba)
SDSSJ0015+0013	6065	6.82 ± 0.17	7.03 ± 0.18	7.82	−0.03	7.28	7.22	5.81/6.01 ± 0.21	4.45 ± 0.20	4.79 ± 0.21		1.74
SDSSJ0040+0025	5651	5.53 ± 0.21		6.53	−0.15	6.02		4.76/4.64 ± 0.18	3.14 ± 0.27	3.62 ± 0.24	0.46	0.54
SDSSJ0042+0055	6019	5.87 ± 0.13		6.79	−0.15	6.34		5.21/5.03 ± 0.15	3.75 ± 0.17	3.77 ± 0.08	1.67	1.35
SDSSJ0222−0313	6345	4.89 ± 0.24		8.08	−0.08			4.11/4.12 ± 0.30	3.17 ± 0.01		2.54	1.52
SDSSJ0309+0542	6012	6.56 ± 0.16	6.36 ± 0.20	7.74	+0.05	7.17		5.71/5.73 ± 0.22	4.42 ± 0.32	4.49 ± 0.14	2.02	1.15
SDSSJ0346−0558	5660	6.67 ± 0.19	6.51 ± 0.19	7.61	+0.10	7.06		5.62/5.55 ± 0.06	4.27 ± 0.25	4.74 ± 0.30	2.00:	1.50
SDSSJ0905+0330	6263	4.40 ± 0.27		7.68	−0.15			3.99/3.52 ± 0.30			0.40:	1.47:
SDSSJ1149+0723	6000	4.7 ± 0.40:		7.66	−0.05			3.86/3.70 ± 0.30		2.50 ± 0.30	<1.0	0.30:
SDSSJ1248−0726	6234	5.88 ± 0.39		7.94	−0.10	6.40		4.99/5.09 ± 0.32	3.62 ± 0.13	4.09 ± 0.30	2.64	3.05
SDSSJ1315+1727	6170	5.00 ± 0.06		8.34	−0.05			3.99			0.30:	1.81
SDSSJ1337+0835	6023	6.21 ± 0.17		7.35	+0.00	6.91		5.38/5.39 ± 0.13	3.74 ± 0.28	4.19 ± 0.18	1.80	0.90
SDSSJ1337+0836	5970	6.74 ± 0.18		8.44	+0.15	7.18		6.27/6.00 ± 0.38	4.32 ± 0.18	4.39 ± 0.30		1.90
SDSSJ1337+0837	5464	7.07 ± 0.25		8.10	+0.15			6.09/6.22 ± 0.24	4.46 ± 0.28	4.88 ± 0.31		1.82
SDSSJ1338+0830	5496	6.99 ± 0.18		8.04	+0.15	7.61		6.02/6.10 ± 0.26	4.72 ± 0.23	4.94 ± 0.24		1.67:
SDSSJ1342+0835	6176	6.04 ± 0.23		7.00:	−0.10			5.21/4.91 ± 0.16	3.89 ± 0.24	3.68 ± 0.30	1.85	0.51
SDSSJ1343+0810	5482	7.02 ± 0.22		7.97	+0.15	7.45	7.37	6.03/6.02 ± 0.07	4.72 ± 0.16	5.33 ± 0.14		1.72
SDSSJ1349−0229	6138	4.5 ± 0.40:		8.32	+0.00			3.78			1.00:	1.50
SDSSJ1411+0503	5930	4.16 ± 0.23		6.86	−0.15			3.91			−0.19	<−0.8
SDSSJ1445−0045,2	5492	4.58 ± 0.19		6.18	−0.15			3.64/3.30 ± 0.30	2.65 ± 0.26		−0.12	<−1.0
SDSSJ1445−0045,1	5492	4.49 ± 0.21		6.18	−0.15			3.63/3.49 ± 0.29	2.53 ± 0.06		−0.34	<−1.0
SDSSJ1543+0929	6288	5.14 ± 0.08		8.42	−0.05			4.05			1.13:	1.21:
SDSSJ1606+0522	6122	6.25 ± 0.29	6.55	7.81	+0.00	6.58		5.38/5.69 ± 0.01	4.59 ± 0.04		3.29	2.95
SDSSJ2137−0057	5956	4.43 ± 0.40		6.70	−0.15			3.73			<−0.5	−0.02
SDSSJ2219+0515	6351	5.3 ± 0.40:		8.36	+0.00			4.11			<0.0	1.40:
SDSSJ2239−0048	6317	6.03 ± 0.22		7.91	−0.05	6.46		5.19/5.07	3.94 ± 0.39		3.31	3.45
SDSSJ2311+0026	5967	5.84 ± 0.27		7.06	−0.10	6.70		5.20/5.03 ± 0.04	3.67 ± 0.07	3.72 ± 0.30	1.77	1.10
SDSSJ2335+0819	5951	6.30 ± 0.19		7.36	+0.05	6.93		5.42/5.32 ± 0.05	4.23 ± 0.36	4.39 ± 0.38	1.70	0.88
SDSSJ2337+1436	5746	6.67 ± 0.23		7.76	+0.10	7.34		5.80/5.79 ± 0.18	4.14 ± 0.34	4.39 ± 0.30		1.45
SDSSJ1114−1202	5879	6.45 ± 0.22		7.61	+0.10	7.18 ± 0.22		5.15:/5.47 ± 0.11	3.87 ± 0.09		1.00:	0.92:
SDSSJ2011−1110	5540	6.49 ± 0.17	6.66 ± 0.07	7.35	+0.10	7.18 ± 0.11	7.13	5.36:/5.45 ± 0.09	4.05 ± 0.21	4.45 ± 0.42	1.84:	1.35
SDSSJ2123−0804	5468	4.61 ± 0.09		6.00	−0.10	5.00 ± 0.13		3.91/3.74 ± 0.34	2.41		0.47:	0.46

Notes. A colon indicates uncertain values.

at the time of the observation, and using the FORS manual indications, we derived the uncertainties in radial velocities. These values are higher than the formal uncertainty in each cross-correlation, and for the majority of the spectra, taking it into account does not change the total uncertainty. For three spectra (for the stars SDSS J2239−0048, SDSS J1248−0726, and SDSS J0905+0330), the formal uncertainty increases the total uncertainty by 1 km s^{-1}, and SDSS J1411+0503, for which the quality of the cross-correlation is worse, still shows a clear peak, and the total uncertainty is increased by 3 km s^{-1}. For the GMOS stars we had no information on the telescope flexions, so that at present we prefer to not provide the radial velocities. Comments on some stars are provided below.

– SDSS J0015+0013 has six SDSS spectra. The metallicities are in very good agreement, with a scatter of 0.06 dex. Of the six radial velocities, five are compatible within the uncertainties, but one is not (−18 ± 2, −24 ± 3, −20 ± 3, −8 ± 3, −19 ± 2, and −18 ± 2). The star is probably a member of a multiple system. Our value of −10 ± 20 lies within the SDSS values, but the uncertainty is large enough to be compatible with any SDSS value.

– SDSS J0346−0558 has three SDSS spectra. Two of them are very similar in metallicity (the average value is listed in Table 1) and agrees within the uncertainties with the FORS analysis, while the third failed the chemical analysis. This failure of this latest spectrum is related to the peculiar value of the radial velocity of −1159 km s^{-1} that is provided. The other two SDSS spectra provide very similar radial velocities values, well within the

SDSS uncertainties, and the average value is provided in Table 1.
– For SDSS J1606+0522, we find a double peak in the cross-correlation at 77 km s^{-1} from the mean peak.
– The difference between the SDSS and the FORS radial velocities in SDSS J1248−0726 is larger than the uncertainties. This can be an indication of a multiple system.
– SDSS J2335+0819 has two SDSS spectra whose radial velocities are in agreement well within the uncertainties. The metallicity derived from the spectra agrees within the uncertainties, but for one of them, the metallicity is based on many more features, with a much smaller uncertainty; we list this result in Table 1.
– For SDSS J2239−0048, three SDSS spectra are available. The metallicities derived from these spectra are in perfect agreement (the average value is provided in Table 1). The radial velocities indicate an object in a multiple system; the three values (−128 ± 4, −141 ± 3, and −145 ± 2) are incompatible with a constant radial velocity. The FORS radial velocity is compatible with any SDSS value.
– The two spectra of SDSS J0042+0055 in SDSS give metallicities and radial velocities in very good agreement. The metallicity is in perfect agreement with [Fe/H] derived from the FORS spectrum, and the radial velocity difference of 14 km s^{-1} is well within the uncertainties.
– The disagreement between the SDSS and FORS radial velocities for SDSS J1411+0503 and SDSS J2137−0057 is just larger than the uncertainties.
– Twelve spectra of SDSS J0040+0025 are available in SDSS.

The metallicities we derived from them are in excellent agreement ($\sigma = 0.04$ dex) and also agree excellently with the [Fe/H] derived from the FORS spectrum. The 12 radial velocities span from 75 to 86 km s^{-1}. The scatter on them is 3 km s^{-1}, which is compatible with the uncertainties, but might indicate a variation in the radial velocity of this star. The radial velocity derived from the FORS spectrum is compatible with the values from the SDSS spectra.

– The radial velocities of the two SDSS spectra of SDSS J1315+1727 agree well and lie well within the uncertainties. They also agree within the uncertainties with the measurement from the FORS spectrum. The two metallicities also agree well and agree with the [Fe/H] from FORS spectrum within the uncertainties.

– The two FORS spectra of SDSS J1445–0045 have radial velocities and [Fe/H] in agreement within the uncertainties, and they both agree with the values from the SDSS spectrum.

– The two SDSS spectra of SDSS J2137–0057 provide extremely good agreement in the metallicities derived and with [Fe/H] derived from the GMOS spectrum, while the radial velocities of -95 ± 5 and -108 ± 5 could indicate a variation (the highest value is reported in Table 1). We were unable to derive a robust radial velocity from the GMOS spectrum.

– The two spectra of SDSS J1349–0229 in SDSS show a difference in radial velocities that is larger than the uncertainties (140 ± 3 and 131 ± 3, the first value is listed in Table 1). The value from the FORS spectrum is compatible with both values.

– The radial velocities derived from the two SDSS spectra of SDSS J1114–1202 are consistent within the uncertainties. We were unable to derive a reliable radial velocity from the GMOS spectrum. Metallicity and [Fe/H] from the SDSS and GMOS spectra agree within uncertainties.

– The two SDSS spectra of SDSS J2011–1110 provide radial velocities that are perfectly consistent. Metallicity and [Fe/H] from the SDSS and GMOS spectra agree within uncertainties.

4.3. Chemical analysis

The stars were selected as turn-off stars, so that we fixed the surface gravity at 4.0 in the analysis. The temperature was derived from the Sloan colours as in Caffau et al. (2013b). To derive the chemical composition, we analysed the spectra with the pipeline MyGIsFOS (Sbordone et al. 2014). The grid of theoretical syntheses were computed with Turbospectrum (Alvarez & Plez 1998; Plez 2012) on a MARCS grid of models (Gustafsson et al. 2008).

After we determined A(Fe), we produced a grid of synthetic spectra with the same Fe content, but various C abundances and fitted the G-band in order to derive A(C). We repeated this to derive A(Ca) from the Ca II-K line and the Sr and Ba abundances. Because of the low resolution of the spectra, we were only able to derive a few elements, but because the Ca II-K line and G-band are so prominent, we were able to derive Ca and C from the G-band from any spectrum. For many spectra, we were also able to derive the abundances of Fe, Ti, Mn, Sr, and Ba. The detailed abundances are reported in Table 2, and in Fig. 1, we show four of the spectra. We have an uncertainty of 0.15 dex in deriving A(Ca) from the Ca II-K line. The A(Ca) derived from the Ca II-K line usually agrees within uncertainties with the value derived from Ca I lines, except for SDSS J1606+0522, SDSS J0905+0330, and SDSS J1114–1202. For the star SDSS J1606+0522, an uncertainty of 0.31 dex is reasonable because of the spectrum quality, but the scatter of
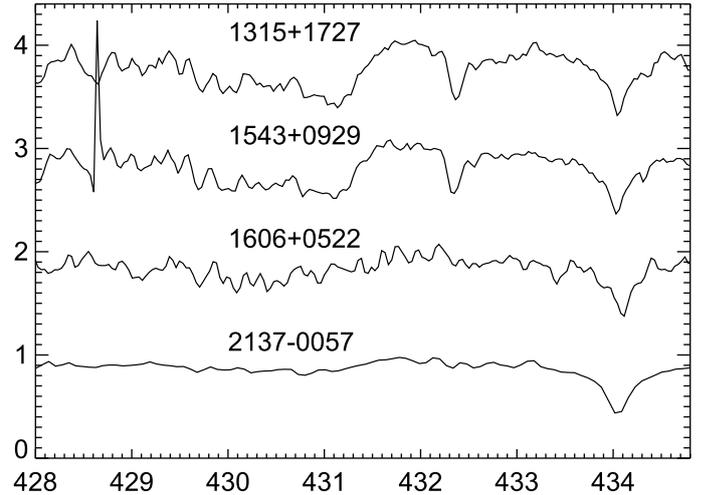
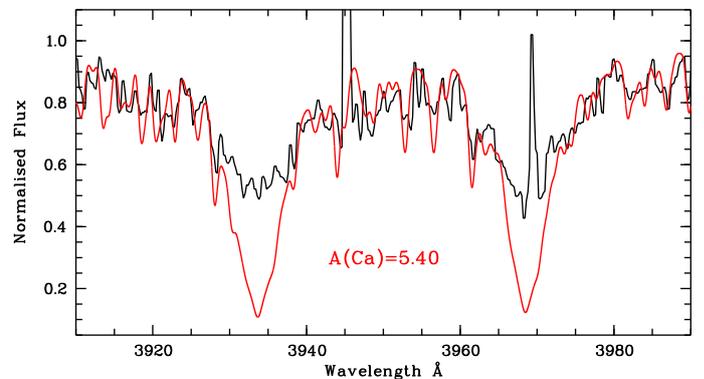**Fig. 1.** Observed spectra for four stars in the range of the G-band.

Fig. 2. Observed spectrum of SDSS J1114–1202 (solid black) compared with a synthetic spectrum (solid red) with A(Ca) compatible with the value derived from the other two Ca I lines and with A(Fe).

0.01 dex among the two Ca I lines is a random chance event. For the star SDSS J0905+0330, the A(Ca) is based on the single Ca I line at 422 nm, which is often in disagreement with the other lines. The star is metal poor, therefore a contamination from the ISM of the Ca II-K could increase the A(Ca) derived from this line. For the star SDSS J1114–1202, the Ca II-K line was clearly too shallow. In Fig. 2 we compare the Ca II-K line with a synthetic spectrum with a Ca abundance compatible with A(Ca) derived from two Ca I lines and consistent with the Fe abundance. The wings of the Ca II-H and -K lines in the synthesis reproduce the observed spectrum very well, while the core of the line is not present. We suspect that this is due to chromospheric emission. The H-lines in the spectrum of this star are also weak.

In Table 2 we also provide a 3D correction on the C abundance as derived from the G-band by Gallagher et al. (2016). The solar A(Fe) used to produce the figures is adopted from Caffau et al. (2011), while the other solar abundances are taken from Lodders et al. (2009).

For two stars, SDSS J1445–0045 and SDSS J0905+0330, we have hydrodynamical models from the CIFIST grid (Ludwig et al. 2009) with parameters very similar to what is observed. We fitted the G bands of these two stars with the synthetic spectra computed using these 3D models with Linfor3D[8] (Gallagher et al. 2017b). The best fits are presented in Figs. 3 and 4. As

---

[8] http://www.aip.de/Members/msteffen/linfor3d
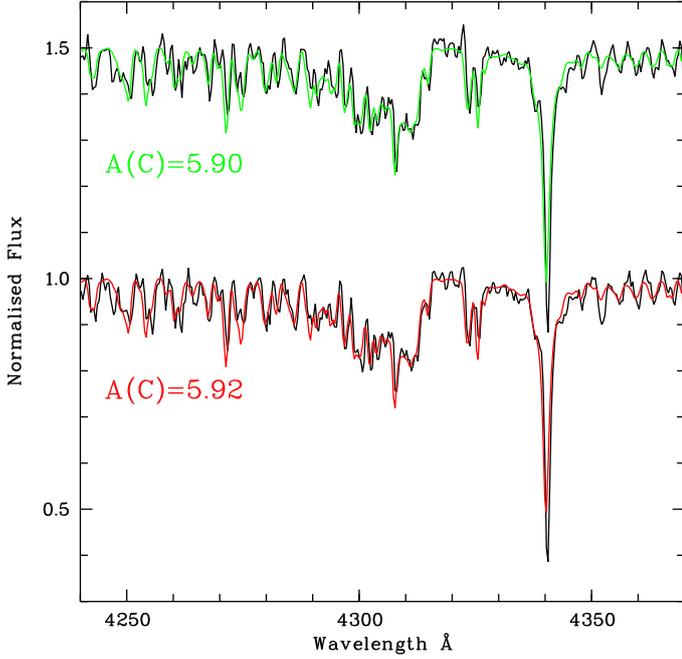
Fig. 3. Two observed spectra of SDSS J1445–0045 (solid black) compared with the best fit (solid green and red) based on a 3D synthesis of a model that is 18 K cooler.
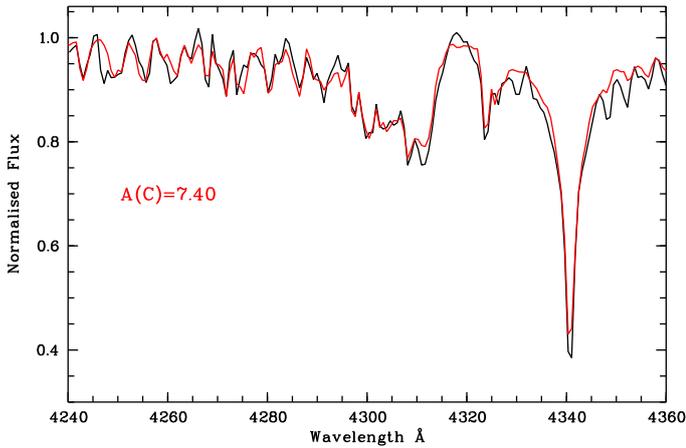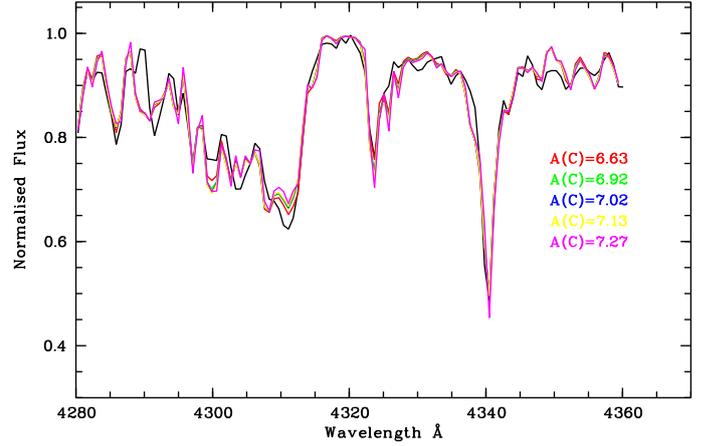

Fig. 4. Observed spectrum of SDSS J0905+0330 (solid black) compared with the best fit (solid red) based on a 3D synthesis of a model that is 21 K cooler.

was explained in Gallagher et al. (2016), the *G*-band is extremely sensitive to changes in the oxygen abundance. Because we were unable to directly measure the oxygen abundance, the 3D syntheses were computed so that oxygen scales with carbon at a consistent ratio corresponding to A(C)–A(O) of –0.67.

4.4. SDSS J1313–0019

In the sample of stars, we also observed SDSS J1313–0019, a star discovered by Allende Prieto et al. (2015) that was later also analysed by Frebel et al. (2015). Both analyses show that the star is an evolved star, extremely low in [Fe/H], with a C content that places the star in the low *C* band.

The goal of the work presented in this paper is not to improve our knowledge of the chemical composition of this star with the FORS spectra. The aim is instead to test the

Fig. 5. Observed spectrum of SDSS J1313–0010 (solid black) compared with the best fit based on a 3D synthesis with various C/O content. The pink profile corresponds to A(C)–A(O) = –1.67, and the red profile shows A(C)–A(O) = +0.33.
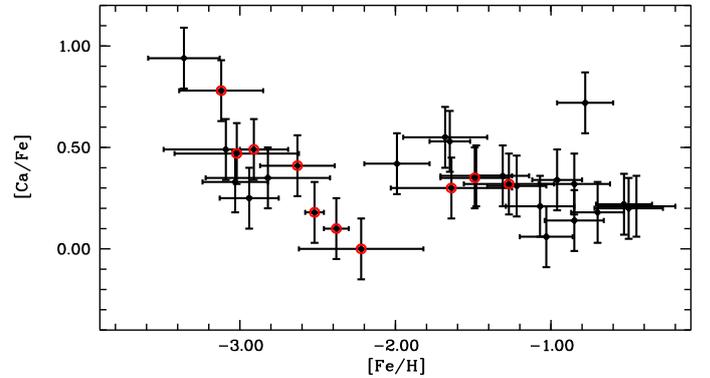

Fig. 6. [Ca/Fe] derived from the Ca II-K line vs. [Fe/H]. The black dots surrounded by a red corona represent Ba-rich stars. The solar A(Fe) value of 7.52 is taken from Caffau et al. (2011), and the solar A(Ca) = 6.33 is adopted from Lodders et al. (2009).
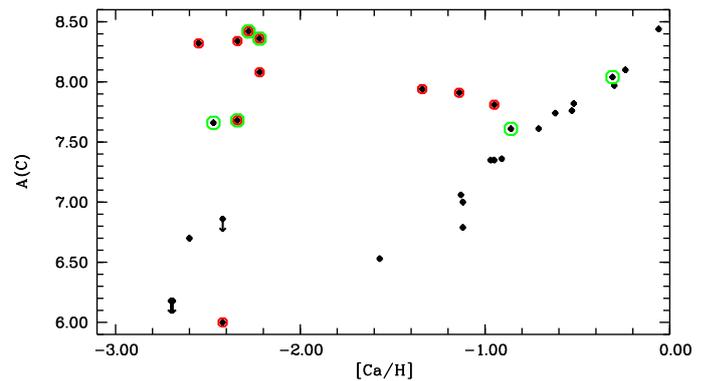
Fig. 7. Carbon abundance vs. [Ca/H] derived from the Ca II-K line. The black dots surrounded by a red corona represent Ba-rich stars. An extra green corona is used in the cases of uncertain measurements. Downward arrows represent upper limits.

3D spectra and observationally verify if the C abundance we derive varies by changing the oxygen abundance simulated in the synthesis. The closest 3D model in the CIFIST grid has parameters $T_{\mathrm{eff}} = 5500$ K, $\log g$ of 2.5 [cgs], and [Fe/H] = –3.0; the model parameters are similar to those suggested by Allende Prieto et al. (2015) (T_{eff} = 5378 K, $\log g$ = 3.0,
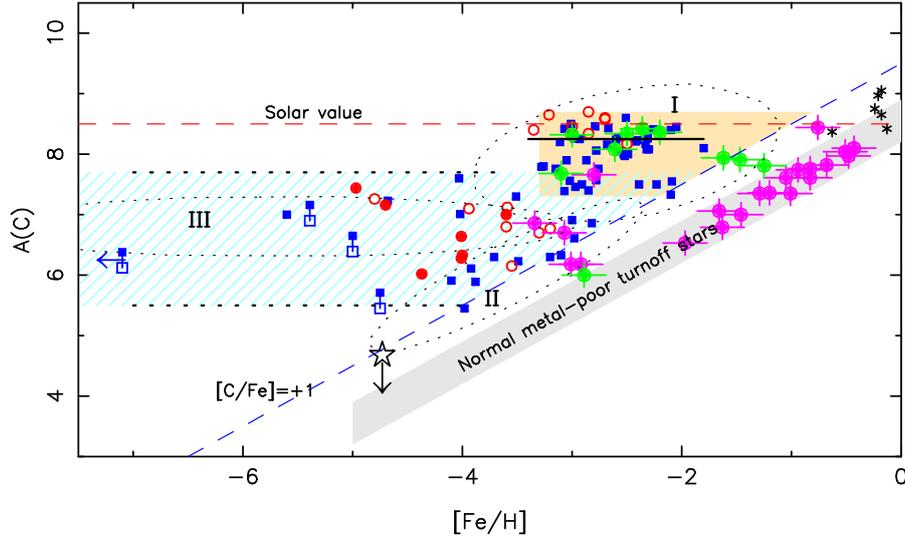
Fig. 8. Carbon abundance vs. [Fe/H] of the sample stars (pink and green dots show stars normal and rich in Ba, respectively). Red solid dots are the stars we analysed in the TOPoS project (Bonifacio et al. 2018); the open red dots are taken from Sivarani et al. (2006); Bonifacio et al. (2009, 2015); Spite et al. (2013); Behara et al. (2010); Sivarani et al. (2004) and Caffau et al. (2013a, 2016); the black star is taken from Caffau et al. (2012). The black asterisks show known CH dwarf stars (Karinkuzhi & Goswami 2014, 2015). The blue squares show stars from the literature (Yong et al. 2013; Cohen et al. 2003, 2013; Carollo et al. 2014; Masseron et al. 2012; Jonsell et al. 2006; Thompson et al. 2008; Hansen et al. 2015, 2016; Lucatello et al. 2003; Aoki et al. 2002, 2006, 2008; Frebel et al. 2005; Li et al. 2015; Norris et al. 2007; Christlieb et al. 2004; Keller et al. 2014; Frebel et al. 2015; Roederer et al. 2014; Ivans et al. 2005). The blue and orange areas in the figure highlight the two carbon bands as defined in Bonifacio et al. (2018). The black dashed ellipses represent the regions containing the three CEMP populations according to Yoon et al. (2016).

[Fe/H] = −4.3, and [C/Fe] = +2.5), with the exception of the iron content. The 3D model was computed with a solar-scaled composition and an enhancement in α-elements of 0.4 dex, typical of a metal-poor star. When computing the synthesis, several C/O ratios were considered. We then fitted the observed profile using a synthesis grid with the same C/O ratio (see Gallagher et al. 2017a, for details). The fit was also made using a grid of 1D LHD models (Caffau & Ludwig 2007), computed with the same C/O ratios. At the typical temperatures, these stars have (5500–6500 K), the A(C) value derived from the 1D fit is not sensitive to changing C/O: a negligible difference of 0.09 dex is found when A(C)–A(O) is varied by up to 2.0. Conversely, the change in the C abundance from the 3D fit is 0.64 dex when A(C)–A(O) is varied by the same amount. When the oxygen abundance is varied for any given carbon abundance, the shape of the G-band varies as well. This is most notable in the band head. However, a higher spectral resolution is required for this effect to be notable. The fits are shown in Fig. 5. The shape of the G-band also changes by changing C/O; the plot appears to favour a lower oxygen, and the χ^2 test also favours this case.

5. Results

In Fig. 6 we show the [Ca/Fe] versus [Fe/H]. The Ca abundance has been derived from the Ca II-K line for this plot, for which we estimated an uncertainty of 0.15 dex, while the uncertainty on Fe is the line-to-line scatter, except for the stars for which no clear Fe line is available; in this case, the uncertainty is related to a comparison with synthetic spectra. The stars, as expected, all seem mostly α-enhanced. The star with the lowest [Ca/Fe] (SDSS J2219+0515) is one with the poorest A(Fe) determination, so that within 1 σ the star is a α-enhanced metal-poor star, at the same level as a typical metal-poor star.

In Fig. 7 the carbon abundance, derived from the G band and listed in Table 2, is plotted as a function of the [Ca/H] ratio, with

the Ca abundance derived from the Ca II-K line. In the figure, the stars with [Fe/H] < −2 are located in the higher part of the plot, which means that they belong to the high C band of Spite et al. (2013) or have a low A(C) value, placing them on the low C band. Interestingly, all the stars in the high C band are rich in Ba (two stars, SDSS J1543+0929 and SDSS J2219+0515, have an uncertain A(Ba) value, which is depicted as a green corona in the figure). The stars belonging to the low C band are not rich in Ba (they have a low [Ba/Fe] or an upper limit): they are CEMP-no stars. Two stars (SDSS J0905+0330 and SDSS J1149+0723) with a very similar A(C) value, just below 7.7, both belong to the higher C band. The latter, SDSS J1149+0723, does not appear to be Ba-rich, but the result, as for the other, is uncertain.

We revisited Fig. 7 by comparing our sample of stars with the literature in Fig. 8. This plot has been devised by Spite et al. (2013) and was recently revisited by Bonifacio et al. (2018), who also suggested a classification of CEMP stars according to C abundance different from the one of Yoon et al. (2016). The blue and orange areas in the figure highlight the two carbon bands as defined in Bonifacio et al. (2018), and the three Yoon groups are delimited by dotted lines. Yoon et al. (2016) adopted [C/Fe] > 0.7 instead of [C/Fe] > +1.0 for the definition of CEMP stars. Moreover, in their Fig. 1, Yoon et al. (2016) also included giant stars. To define our two regions (orange and blue) in about the same sample of stars, we kept only dwarfs and turn-off stars where the carbon abundance is not affected by mixing. However, at very low metallicity ([Fe/H] < −4.5), we added four giant stars of the low red giant branch, but all with log g > 2.2. For these stars the correction of the carbon abundance due to the first dredge-up is small and has been estimated from Bonifacio et al. (2009). As visible in Fig. 8, the two regions I and III defined in Yoon et al. (2016) are included in our orange and blue areas (as in Bonifacio et al. 2018), respectively, while stars in region II are either in our low C band (blue area) or are C-normal, according to our definition. In our interpretation, all C-enhanced stars ([C/Fe] > +1.0 as defined in the introduction)
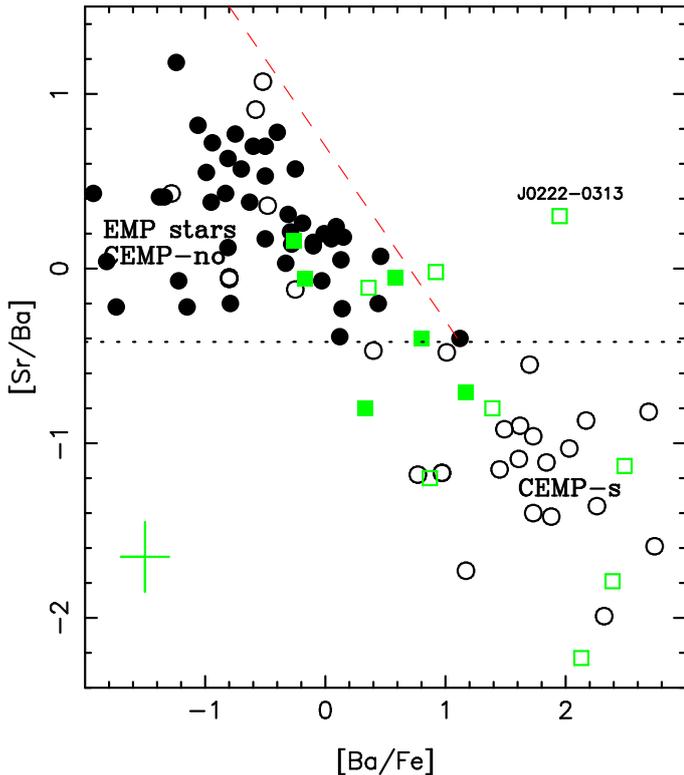
Fig. 9. [Sr/Ba] ratio vs. [Ba/Fe]. The black filled circles represent the normal EMP dwarfs and giants studied in the frame of the ESO Large Programme First Stars (Cayrel et al. 2004; Bonifacio et al. 2009) and the stars studied homogeneously by Siqueira-Mello et al. (2015). The black open circles are for CEMP stars studied in the frame of this ESO Large Programme or taken from the literature (Depagne et al. 2002; Sivarani et al. 2004, 2006; Barbuy et al. 2005; Behara et al. 2010; Spite et al. 2013; Yong et al. 2013). The green filled squares show normal metal-poor stars studied in this paper, and the open green squares denote the C-rich stars. Note the very peculiar position of the CEMP star SDSS J0222–0313. In this star the first-peak heavy elements (such as Sr) seem to be more enriched than the second-peak heavy elements (like Ba).

in the figure are adequately accounted for by the high and low *C* bands (as defined in Bonifacio et al. 2018). The stars analysed here are shown in Fig. 8 as pink (normal in Ba) and green (Ba rich) filled dots, in comparison with other stars taken from the literature. The stars lying below the blue dashed line are carbon-normal stars. In this figure the CEMP ([Fe/H] < −2.0) Ba-rich stars clearly belong to the high *C* band, while the stars with normal Ba are part of the low *C* band. The two stars SDSS J0905+0330 and SDSS J1149+0723, one normal and one rich in Ba, but with uncertain measurements, are also similar in [Fe/H] and are placed in the lower part of the high *C* band or in the upper part of the low *C* band.

In Fig. 9 we compare the position of the most metal-poor stars in our sample ([Fe/H] < −1.5) with a sample of metal-poor stars collected from the literature, which are, in general, slightly more metal poor than our sample. They are depicted in the form [Sr/Ba] vs. [Ba/Fe]. These stars are generally slightly more metal poor than our sample ([Fe/H] < −2.5). The "normal" stars (i.e. not C-rich) are represented by filled symbols and the C-rich stars ([C/Fe] > 1.0) by open symbols. The green square symbols represent the stars studied in this paper and the black circles show the stars taken from the literature. In normal metal-poor stars, [Sr/Ba] is higher than –0.4, a value observed in particular in the

stars that are strongly enriched in neutron-capture elements, such as CS31082-001, which is explained by a pure r-process enrichment and is classified as "r II". The stars SDSS J2123–0804 and SDSS J0042+0055 could also belong to this class when we take the uncertainties into account.

In Fig. 9 several carbon-rich stars are located in the same region as the "normal" metal-poor stars (CEMP-no). Many CEMP stars are enriched in heavy elements (CEMP-s or -r/s), however, such as in general [Ba/Fe] > 1 and [Sr/Ba] < −0.4; the second peak of the neutron-capture elements such as Ba is more enriched than the first-peak elements such as Sr. SDSS J0222–0313 is characterised by a high value of [Ba/Fe] ([Ba/Fe] = 1.95) and an even higher value of [Sr/Fe] ([Sr/Fe] = 2.25). The high abundance of Sr is also confirmed by the Sr II line at 421.55 nm. In this star the yttrium line (another first-peak neutron-capture element) at 395.04 nm was also detected and measured: [Y/Fe] = +2.57. It would be interesting to be able to measure more neutron-capture elements in this star to explain its unexpected abundance pattern.

6. Conclusions

We analysed 30 unevolved stars and reinvestigated one known ultra Fe-poor star (Allende Prieto et al. 2015). In spite of the low resolution of the spectra, we were able to derive very useful information to better understand the C-enhanced stellar population. The CEMP stars belonging to the high *C* band are enhanced in Ba, while those belonging to the low band show a normal A(Ba) value. This finding supports the idea of Bonifacio et al. (2015) that the high band is populated by binary stars and the high abundances are the result of mass-transfer from a companion, while the stars of the low band, with normal A(Ba), formed from a C-rich gas cloud.

We compared the [Sr/Ba] ratio as a function of [Ba/Fe] for the most Fe-poor stars of this sample to a more metal-poor sample. In Fig. 9, our stars appear to be similar to the most metal-poor population; the Ba normal stars are mainly clustered in the upper left side of the diagram and the Ba-rich stars lie in the lower right side. One star, SDSS J0222–0313, is alone in the upper right part of the plot. We need high-resolution observation for this star to confirm with a higher degree of certainty that the first-peak elements (here Sr and Y) are more abundant with respect to Fe than those of the second peak (here Ba).

We also investigated the *G*-band of the known giant star (Allende Prieto et al. 2015) using a synthesis computed from a hydrodynamical model with parameters similar to those of the star. Because according to the 3D theoretical computation, the shape of the *G*-band changes as a function of the C/O ratio, we might place constraints on the oxygen abundance by fitting the *G*-band. In the case of SDSS J1331–0019, a [O/Fe] lower than [C/Fe] is expected. Spectra with a higher resolution would be needed to confirm this, however.

References

Allende Prieto, C., Fernández-Alvar, E., Aguado, D. S., et al. 2015, A&A, 579, A98
Alvarez, R., & Plez, B., 1998, A&A 330, 1109
Aoki, W., Ryan, S. G., Norris, J. E., et al. 2002, ApJ, 580, 1149

Aoki, W., Frebel, A., Christlieb, N., et al. 2006, ApJ, 639, 897
Aoki, W., Beers, T. C., Christlieb, N., et al. 2007, ApJ, 655, 492
Aoki, W., Beers, T. C., Sivarani, T., et al. 2008, ApJ, 678, 1351
Appenzeller, I., Fricke, K., Fürtig, W., et al. 1998, The Messenger, 94, 1
Barbuy, B., Cayrel, R., Spite, M., et al. 1997, A&A, 317, L63
Barbuy, B., Spite, M., Spite, F., et al. 2005, A&A, 429, 1031
Beers, T. C., & Christlieb, N. 2005, ARA&A, 43, 531
Beers, T. C., Preston, G. W., & Shectman, S. A. 1985, AJ, 90, 2089
Beers, T. C., Preston, G. W., & Shectman, S. A. 1992, AJ, 103, 1987
Behara, N. T., Bonifacio, P., Ludwig, H.-G., et al. 2010, A&A, 513, A72
Bidelman, W. P. 1956, Vist. Astron., 2, 1428
Bisterzo, S., Gallino, R., Straniero, O., et al. 2006, Mem. Soc. Astron. It., 77, 985
Bonifacio, P., Molaro, P., Beers, T. C., & Vladilo, G. 1998, A&A, 332, 672
Bonifacio, P., Spite, M., Cayrel, R., et al. 2009, A&A, 501, 519
Bonifacio, P., Caffau, E., Spite, M., et al. 2015, A&A, 579, A28
Bonifacio, P., Caffau, E., Spite, M., et al. 2018, A&A, 612, A65
Caffau, E., & Ludwig, H.-G. 2007, A&A, 467, L11
Caffau, E., Ludwig, H.-G., Steffen, M., Freytag, B., & Bonifacio, P. 2011, Sol. Phys., 268, 255
Caffau, E., Bonifacio, P., François, P., et al. 2012, A&A, 542, A51
Caffau, E., Bonifacio, P., François, P., et al. 2013a, A&A, 560, A15
Caffau, E., Bonifacio, P., Sbordone, L., et al. 2013b, A&A, 560, A71
Caffau, E., Bonifacio, P., Spite, M., et al. 2016, A&A, 595, L6
Carollo, D., Freeman, K., Beers, T. C., et al. 2014, ApJ, 788, 180
Cayrel, R., Depagne, E., Spite, M., et al. 2004, A&A, 416, 1117
Christlieb, N. 2003, Rev. Mod. Astron., 16, 191
Christlieb, N., Gustafsson, B., Korn, A. J., et al. 2004, ApJ, 603, 708
Cohen, J. G., Christlieb, N., Qian, Y.-Z., & Wasserburg, G. J. 2003, ApJ, 588, 1082
Cohen, J. G., Christlieb, N., Thompson, I., et al. 2013, ApJ, 778, 56
Cowan, J. J., & Rose, W. K. 1977, ApJ, 212, 149
Depagne, E., Hill, V., Spite, M., et al. 2002, A&A, 390, 187
Frebel, A., Aoki, W., Christlieb, N., et al. 2005, Nature, 434, 871
Frebel, A., Chiti, A., Ji, A. P., Jacobson, H. R., & Placco, V. M. 2015, ApJ, 810, L27
Gaia Collaboration (Brown, A. G. A., et al.) 2016, A&A, 595, A2
Gallagher, A. J., Caffau, E., Bonifacio, P., et al. 2016, A&A, 593, A48
Gallagher, A. J., Caffau, E., Bonifacio, P., et al. 2017a, A&A, 598, L10
Gallagher, A. J., Steffen, M., Caffau, E., et al. 2017b, Mem. Soc. Astron. It., 88, 82
Gimeno, G., Roth, K., Chiboucas, K., et al. 2016, Proc. SPIE, 9908, 99082S
Gustafsson, B., Edvardsson, B., Eriksson, K., et al. 2008, A&A 486, 951
Hampel, M., Stancliffe, R. J., Lugaro, M., & Meyer, B. S. 2016, ApJ, 831, 171
Hansen, T., Hansen, C. J., Christlieb, N., et al. 2015, ApJ, 807, 173
Hansen, T. T., Andersen, J., Nordström, B., et al. 2016, A&A, 588, A3
Hook, I. M., Jørgensen, I., Allington-Smith, J. R., et al. 2004, PASP, 116, 425

Ivans, I. I., Sneden, C., Gallino, R., Cowan, J. J., & Preston, G. W. 2005, ApJ, 627, L145
Jonsell, K., Barklem, P. S., Gustafsson, B., et al. 2006, A&A, 451, 651
Karinkuzhi, D., & Goswami, A. 2014, MNRAS, 440, 1095
Karinkuzhi, D., & Goswami, A. 2015, MNRAS, 446, 2348
Keller, S. C., Bessell, M. S., Frebel, A., et al. 2014, Nature, 506, 463
Li, H.-N., Zhao, G., Christlieb, N., et al. 2015, ApJ, 798, 110
Lodders, K., Palme, H., & Gail, H.-P. 2009, in Landolt-Börnstein - Group VI Astronomy and Astrophysics Numerical Data and Functional Relationships in Science and Technology, ed. J. E. Trümper, (Berlin: Springer-Verlag), 4B, 560
Lucatello, S., Gratton, R., Cohen, J. G., et al. 2003, AJ, 125, 875
Lucatello, S., Tsangarides, S., Beers, T. C., et al. 2005, ApJ, 625, 825
Ludwig, H.-G., Caffau, E., Steffen, M., et al. 2009, Mem. Soc. Astron. It., 80, 711
Masseron, T., Johnson, J. A., Lucatello, S., et al. 2012, ApJ, 751, 14
McCarthy, M. F. 1994, The MK Process at 50 Years: A Powerful Tool for Astrophysical Insight, eds. C. J. Corbally, R. O. Gray, & R. F. Garrison, ASP Conf. Ser., 60, 224
McClure, R. D. 1984, PASP, 96, 117
McClure, R. D. 1997, PASP, 109, 536
McClure, R. D., & Woodsworth, A. W. 1990, ApJ, 352, 709
McWilliam, A., Preston, G. W., Sneden, C., & Searle, L. 1995, AJ, 109, 2757
Norris, J. E., Ryan, S. G., & Beers, T. C. 1997a, ApJ, 488, 350
Norris, J. E., Ryan, S. G., & Beers, T. C. 1997b, ApJ, 489, L169
Norris, J. E., Christlieb, N., Korn, A. J., et al. 2007, ApJ, 670, 774
Plez, B. 2012, Astrophysics Source Code Library [record ascl: 1205.004]
Roederer, I. U., Preston, G. W., Thompson, I. B., Shectman, S. A., & Sneden, C. 2014, ApJ, 784, 158
Sbordone, L., Caffau, E., Bonifacio, P., & Duffau, S. 2014, A&A, 564, A109
Secchi, A. 1868, Sugli spettri prismatici delle stelle fisse (Roma: Trip. Belle Arti), 11
Siqueira-Mello, C., Andrievsky, S. M., Barbuy, B., et al. 2015, A&A, 584, A86
Sivarani, T., Bonifacio, P., Molaro, P., et al. 2004, A&A, 413, 1073
Sivarani, T., Beers, T. C., Bonifacio, P., et al. 2006, A&A, 459, 125
Sneden, C., McWilliam, A., Preston, G. W., et al. 1996, ApJ, 467, 819
Spite, M., Caffau, E., Bonifacio, P., et al. 2013, A&A, 552, A107
Starkenburg, E., Shetrone, M. D., McConnachie, A. W., & Venn, K. A. 2014, MNRAS, 441, 1217
Thompson, I. B., Ivans, I. I., Bisterzo, S., et al. 2008, ApJ, 677, 556
Troja, E., Piro, L., van Eerten, H., et al. 2017, Nature, 551, 71
Wallerstein, G. 1973, ARA&A, 11, 115
Yanny, B., Rockosi, C., Newberg, H. J., et al. 2009, AJ, 137, 4377
Yong, D., Norris, J. E., Bessell, M. S., et al. 2013, ApJ, 762, 26
Yoon, J., Beers, T. C., Placco, V. M., et al. 2016, ApJ, 833, 20
York, D. G., Adelman, J., Anderson, J. E., et al. 2000, AJ, 120, 1579